NREL
NATIONAL RENEWABLE ENERGY LABORATORY

Rotational Augmentation on a 2.3 MW Rotor Blade with Thick Flatback Airfoil Cross-Sections

Preprint

S. Schreck and L. Fingersh
National Renewable Energy Laboratory

K. Siegel, M. Singh, and P. Medina
Siemens Energy, Inc.

To be presented at the 51st AIAA Aerospace Sciences Meeting
Grapevine, Texas
January 7-10, 2013

Conference Paper
NREL/CP-5000-57372
January 2013

Contract No. DE-AC36-08GO28308

Rotational Augmentation on a 2.3-MW Rotor Blade with Thick Flatback Airfoil Cross Sections

S. Schreck and L. Fingersh
NREL's National Wind Technology Center, 15013 Denver West Parkway, Golden, CO 80401

K. Siegel, M. Singh and P. Medina
Siemens Energy, Inc., 1050 Walnut Street, Suite 303, Boulder, CO 80302

Rotational augmentation was analyzed for a 2.3-MW wind turbine that was equipped with thick flatback airfoils at inboard radial locations and extensively instrumented for acquisition of time varying surface pressures. Mean aerodynamic force and surface pressure data were extracted from an extensive field test database, using stringent criteria for wind inflow and turbine operating conditions. Analyses of these data showed pronounced amplification of aerodynamic forces and significant enhancements to surface pressures in response to rotational influences, relative to two-dimensional, stationary conditions. Rotational augmentation occurrence and intensity in the current effort was found to be consistent with that observed in previous research. Notably, elevated airfoil thickness and flatback design did not impede rotational augmentation.

Nomenclature

c	=	blade chord (m)
c_p	=	surface pressure coefficient
C_n	=	normal force coefficient
C_t	=	tangential force coefficient
D	=	rotor diameter (m)
f	=	frequency (Hz)
Hz	=	Hertz
h	=	height above ground (m)
IEC	=	International Electrotechnical Commission
MW	=	megawatt
r	=	radial location (m)
R	=	blade tip radius (m)
α	=	angle of attack (deg)

I. Introduction

Horizontal axis wind turbines (HAWTs) experience large aerodynamic loads on a routine basis. Elevated aerodynamic loads impose high stresses on major components, and can produce torque variations that adversely impact power quality. These and other factors arising from large, unpredicted aerodynamic loads drive up the overall cost of energy. More thorough understanding of wind turbine aerodynamics will facilitate improved accuracy in wind turbine aerodynamics models, which will enable continued reductions in cost of energy.

Rotational augmentation is incompletely characterized and understood. The widely cited experiments of Himmelskamp[1] showed that stall delay and lift enhancement due to rotation occur on aircraft propellers. To explain these results, radial thinning and chordwise acceleration of the steady boundary layer caused by centrifugal forces and the Coriolis effect were postulated. A complementary theoretical analysis was performed by Banks and Gadd[2] for steady laminar boundary layers on a rotating blade at small incidence. They concluded that rotational effects could stabilize the boundary layer against separation, if the linear adverse external velocity gradient is sufficiently small.

Subsequent experimental and analytical research has been conducted in the rotorcraft field. McCroskey and Yaggy[3] conducted a theoretical analysis for quasi-steady rotor blade flows with small crossflows. For zero or favorable chordwise pressure gradient, the effects of crossflow due to rotor rotation were judged beneficial, especially in regions of incipient separation. However, the effects of crossflow due to rotor rotation were considered to be of smaller magnitude than the effects of crossflows caused by rotor translation. It was also speculated that, in strong adverse pressure gradients, the rotationally induced crossflows played a more influential role. Further rotor experiments[4] suggested that centrifugal forces move the fluid significantly outward in separated regions, but are relatively unimportant regarding aerodynamic force augmentation under these conditions.

More recent HAWT experiments employing surface pressure measurements reached differing conclusions regarding the impact of blade crossflows. Using test data, Madsen and Christensen[5] concluded that rotational effects are of minor importance compared to the influences of aspect ratio and radial pressure gradient. Two other experiments conducted in wind tunnels arrived at different conclusions. Using two-dimensional airfoil performance as a baseline, Barnsley and Wellicome[6] stated that the combination of rotational and three-dimensional effects appeared to suppress the loss of leading edge suction across the entire span, compared to two-dimensional behavior. Ronsten[7] used nonrotating blade data as a baseline and noted that rotation generated significant differences in lift behavior only at the pressure measurement station farthest inboard on the blade.

Using full-scale HAWT data acquired in a wind tunnel, Schreck and Robinson[8] concluded that rotational augmentation was not driven by Reynolds number, prominent global unsteadiness, or sweep effects. Rather, it was associated with distinctive chordwise and radial pressure signatures that varied in an orderly manner in response to changes in radial location and inflow conditions. Subsequent work[9] exploited rotating blade surface pressure data to characterize boundary layer separation and shear layer impingement, and flow field structure evolution with rotational augmentation of the flow field. Closely related research[10,11] correlated experimentally and computationally derived surface flow topologies for the rotating blade, finding excellent agreement and significantly generalizing comprehension of the flow field. Other work[12] isolated tip speed ratio as in independent variable and quantified the influence of tip speed ratio on aerodynamic forces and underlying flow field structure. In addition, flow structure sources of unsteadiness in rotational augmented flows have been experimentally identified and characterized for a bounded set of operating conditions.[13] Related work has quantified key relationships that link mean structure and unsteadiness intensity in rotationally augmented flows, and quantitatively determined that the intensity of aerodynamic force unsteadiness can exceed that elicited by atmospheric turbulent inflows of maximal intensity as specified in design standards.[14] In addition, analyses of rotationally augmented flow fields using spectral decompositions have furnished unique information regarding shedding kinematics.[15]

To date, the principal structures and interactions underlying blade rotational augmentation have been characterized in some detail for subscale geometries, and comprehension has greatly improved. However, rotational augmentation has not been explored in detail for utility-scale turbines. In particular, the occurrence and prominence of rotational augmentation in connection with thick and flatback airfoils has not been examined. The current work addresses this shortfall by analyzing field experiment data acquired from the Siemens 2.3-MW turbine at the National Renewable Energy Laboratory's (NREL's) National Wind Technology Center.

II. Experimental Methods

A. Wind Inflow Measurements

Aerodynamic inflow data presented in this paper were acquired from an 80-m meteorological tower approximately 2.5 rotor diameters (D) upwind of the turbine at NREL's National Wind Technology Center. This tower is instrumented with one sonic anemometer, four levels of cup anemometers and directional vanes, and two levels of temperature and barometric pressure sensors. For this project, turbine hub height instrumentation was IEC-Class. This included an IEC Class-1 cup at a height of 80 m and another at 78.5 m along with a vane at that level. A barometric pressure sensor and temperature sensor were installed immediately below that. The meteorological tower data acquisition system acquired data continuously at a sampling frequency of 20 Hz. To accurately characterize the atmospheric boundary layer, as well as the inflow across the turbine rotor, a 135-m meteorological tower was installed approximately two rotor diameters upwind of the turbine in the dominant wind direction. The 135-m tower was equipped with six levels of cup anemometers and directional vanes, six levels of sonic anemometers with three-axis accelerometers, four levels of temperature sensors, a barometric pressure sensor, and a precipitation sensor. All of these sensors were placed at different heights between 3 m and 134 m above ground. The inflow sensor array is documented in greater detail in ref. 16.

B. Blade and Probe Pressure Measurements

To obtain surface pressure data, one of the Siemens 2.3-MW turbine blades was extensively instrumented to acquire surface pressure measurements at nine radial locations. Each of the nine radial locations had approximately 60 surface pressure taps that were distributed over the suction and pressure surfaces. Pressure tap placement was governed by anticipated pressure distributions and the need to validate both aeroelastic and computational fluid dynamics (CFD) models. Figure 1 shows the nine radial locations on the blade for pressure measurements. At the 7-m and 13-m radial stations, the blade airfoil sections were approximately 60% and 40% thick, and both had flatback configurations.

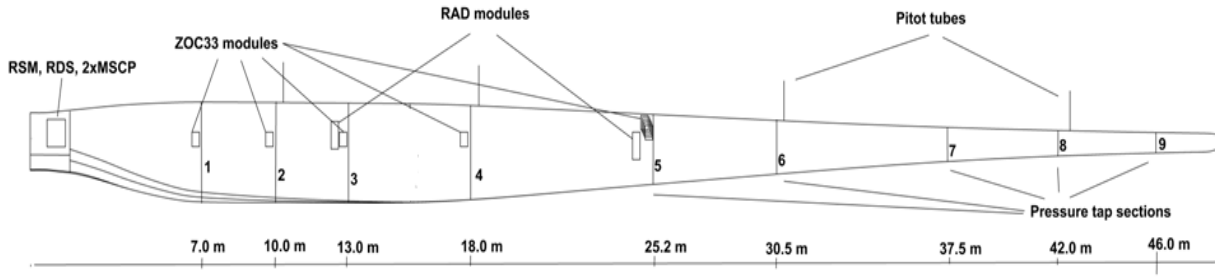

Figure 1. Planform view schematic of Siemens 2.3 MW pressure measurement blade.

The surface pressures at each of these stations were acquired using a combination of Scanivalve ZOC33 and ERAD-4000 modules, discretized at 25 Hz, and transmitted wirelessly to a remote computer for storage and post-processing. To avoid sensor drifts due to temperature variations, the pressure modules were housed in temperature control units (TCU) that maintained the temperatures of the modules at 25° C. Additionally, to reduce the maximum rotational acceleration of the pressure sensors, all the instruments were mounted inside the 25-m blade radius and aligned appropriately as specified by the manufacturer.

Four five-hole probes, also shown in Figure 1, were installed to measure local inflow angles and velocities. These probes extended approximately 0.6 m ahead of the blade leading edge. The setup for five-hole probe data acquisition was essentially the same as that described for the blade surface pressure measurements. Both blade and probe pressure data were post-processed to correct for the effects of hydrostatic pressure variation and reference static pressure deviation. Surface pressure data were integrated over the blade section surface to obtain normal force coefficient (C_n) and tangential force coefficient (C_t) data. Blade and probe pressure instrumentation and data processing procedures were previously documented.[16]

Because of the spatial extent of the blade, tubing lengths between the surface pressure taps and the Scanivalve sensors frequently were of significant length, and pressure signals underwent corresponding distortions. To compensate for these effects, a Wiener inverse filter based on tubing geometry, local temperature, and local pressure was constructed. This inverse filter was applied to measured data to compensate for the extended tubing lengths and to reconstruct the original signal.[17]

III. Results and Discussion

A. Aerodynamics Database and Filtering

The Siemens 2.3-MW turbine field experiment database contained 1987 ten-minute data sets discretized at 25 Hz. These were acquired over a six-month period for a broad range of wind inflow and turbine operating states. To isolate those data for which rotational augmentation was present and that significantly impacted rotor operation, the following filtering procedure was used to extract data from the database.

First, all of the ten-minute data sets were segmented into one-minute data sets. One-minute analysis periods were short enough to avoid averaging out wind inflow conditions and turbine operating responses of interest. At the same time, one-minute periods were long enough to retain a degree of correlation between inflow and turbine data. For each of these one-minute data sets, averages were computed for several inflow and turbine operating parameters, and one-minute data sets were chosen for the current study according to the following filtering criteria.

To ensure that the turbine was operating at a controlled tip speed ratio, blade pitch angle was required to be less than 70°, wind speed required to be 4 m/s or higher, and net power generation required to be positive. In addition, yaw error needed to be between -10° and +10°, to approximate axisymmetric conditions in which rotational

augmentation dominates blade aerodynamics. Finally, wind direction had to be between -20° and +20° of meteorological tower azimuth with respect to the turbine, so that winds impinging on the turbine were the same winds measured by the inflow instrumentation.

Application of these filtering criteria to the 19,870 one-minute data sets identified 157 one-minute data sets that were analyzed in the current study. That less than 1% of all one-minute data sets met the filtering criteria is consistent with the stringent criteria and high turbulence environment at the National Wind Technology Center.

One-minute average wind speed data were binned at 1 m/s intervals and plotted as a histogram in Figure 2. Figure 2 shows that average wind speeds for the 157 one-minute data sets ranged from 4 m/s to 17 m/s. Most one-minute average wind speeds were in the 4 m/s to 13 m/s range, corresponding closely to the Region 2 operating range for the Siemens 2.3-MW turbine. Average wind speeds in the 14 m/s to 17 m/s range, in Region 3, occurred only three times. Overall, the distribution of one-minute wind speeds was skewed slightly to lower wind speeds, with the mean across the 157 one-minute wind speeds being 7.7 m/s, and the mode of 30 realizations occurring at 6 m/s.

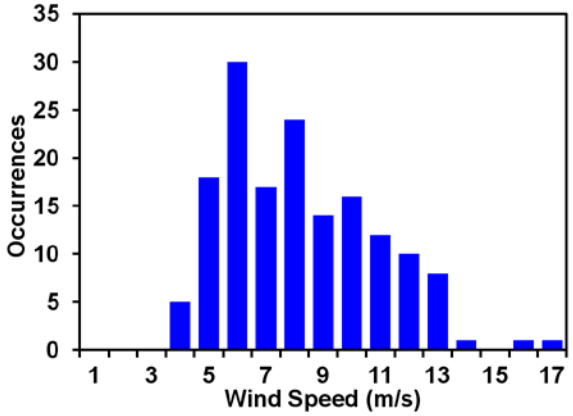

Figure 2. Wind speed histogram for 157 one-minute data files used in the current study.

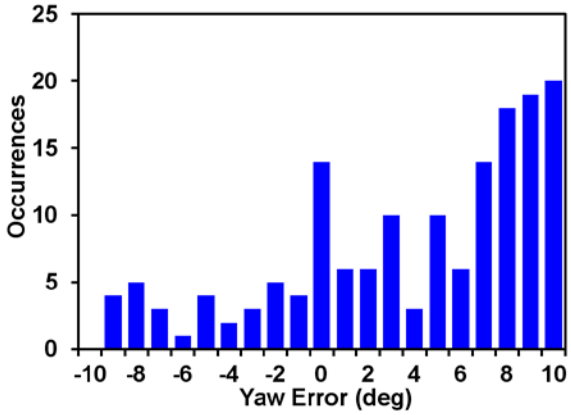

Figure 3. Yaw error histogram for 157 one-minute data files used in the current study.

Average yaw error data for the 157 one-minute data sets were binned at 1° intervals and are plotted as a histogram in Figure 3. Again, approximate axisymmetric conditions were important to the current study, to provide conditions in which rotational augmentation dominates blade aerodynamics. Mean one-minute yaw error realizations occupied bins from -9° to 10°. Mean one-minute yaw error across 157 data sets was 3.4°, and 67 of the 157 data sets had average yaw errors between -5° and 5° (inclusive). However, yaw error realizations were visibly skewed to higher yaw error, with 71 of the one-minute averages lying between 7° and 10° (inclusive).

B. Normal and Tangential Forces

Accompanying the wind inflow data described above in the one-minute data sets were blade surface pressure data. Blade surface pressures were measured at each of the nine radial locations and were discretized at f = 25 Hz. Blade surface pressure data were integrated over the blade surface at each of the nine radial locations to yield time records of C_n and C_t. As shown in Figure 4, C_n is directed perpendicular to the local chord line and is positive pointing outward from the suction surface. C_t is directed parallel to the local chord line and is positive pointing aft from the trailing edge.

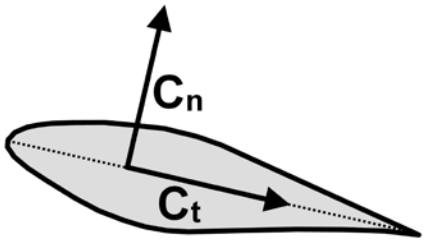

Figure 4. C_n and C_t orientation.

For the current study, C_n and C_t time records for each of the 157 data sets were averaged over the one-minute record to obtain one-minute average data. Typical one-minute average C_n and C_t data for the 7.0 m and 13.0 m blade radius locations are shown in Figures 5 and 6, with $-C_t$ as the abscissa and C_n as the ordinate. Here, these data are plotted as blue circles, with each circle corresponding to one of the 157 one-minute averages.

A two-dimensional, nonrotating reference datum was needed against which three-dimensional, rotational influences associated with rotational augmentation could be assessed. These two-dimensional, nonrotating data were produced using CFDs for airfoil envelopes corresponding to sectional cuts through the blade at the pressure tap rows. These data are represented by the red squares in Figures 5 and 6.

Figure 5 (7-m blade radius) shows that force coefficient levels measured on the rotating blade ranged from ($-C_t$, C_n) = (–0.14, –0.77) at the low end of the point distribution to ($-C_t$, C_n) = (1.21, 2.78) at the upper extreme of the distribution. Though the ensemble of points corresponds to a range of wind speeds (Figure 2) and yaw errors (Figure 3), it is worth noting that the 157 points are organized in an approximately linear region. However, also noticeable for the data point ensemble is the contrast between the tighter, denser point distribution near the lower end and the broader, sparser spread near the upper end. It should be noted that instantaneous C_n and $-C_t$ magnitudes (not documented herein) exceeded the one-minute average data plotted in Figure 5.

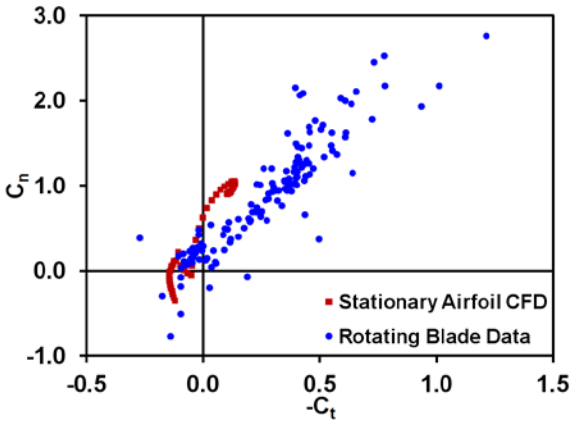

Figure 5. 7-m blade radius C_n vs. $-C_t$ for two-dimensional stationary airfoil CFD (red squares) and three-dimensional rotating blade data (blue circles).

Also shown in Figure 5 (7 m blade radius) are force coefficients computed for two-dimensional, stationary conditions using a fully turbulent boundary layer. The airfoil section used in these computations corresponded to that of the blade section at the tap distribution. Force coefficients ranged from ($-C_t$, C_n) = (–0.12, –0.35) at the low end of the airfoil curve to ($-C_t$, C_n) = (0.13, 1.06) at the upper extreme. The three-dimensional, rotating blade ($-C_t$, C_n) data deviated visibly from the two-dimensional, stationary airfoil ($-C_t$, C_n) point distribution, with the slope of the blade data distribution being visibly lower than that for the airfoil. Most importantly, because of rotational augmentation effects, maximum rotating blade C_n (C_n = 2.78) exceeded maximum stationary airfoil C_n (C_n = 1.06) by a factor of 2.62.

In Figure 6 (13-m blade radius), rotating blade force coefficients ranged from ($-C_t$, C_n) = (–0.21, –0.78) at the lower part of the point distribution to ($-C_t$, C_n) = (0.77, 2.17) at the upper region. It is worth noting that the ensemble of 157 points is approximately linear in shape, even though these data points represent a spectrum of wind speeds (Figure 2) and yaw errors (Figure 3). In the lower part of the point ensemble, the distribution tends to be more condensed, while the upper portion tends to be more expansive. Notably, instantaneous C_n and $-C_t$ magnitudes were greater than the one-minute average data in Figure 6.

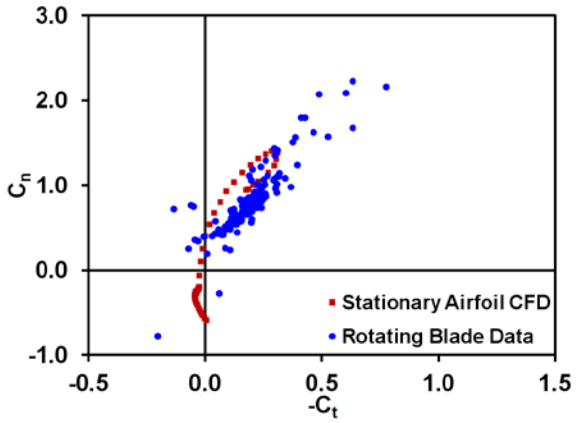

Figure 6. 13 m blade radius C_n vs. $-C_t$ for two-dimensional stationary airfoil CFD (red squares) and three-dimensional rotating blade data (blue circles).

Figure 6 also contains C_n and $-C_t$ predicted by CFD for a two-dimensional, stationary airfoil with a fully turbulent boundary layer. The airfoil section used in these computations was that of the blade section at the 13-m blade radius tap distribution. Force coefficients ranged from ($-C_t$, C_n) = (0.00, –0.59) at the curve lower end to ($-C_t$, C_n) = (0.39, 1.41) at the upper extreme. The two-dimensional, stationary airfoil ($-C_t$, C_n) data deviated from the three-dimensional, rotating blade ($-C_t$, C_n) point distribution, with the slope of the stationary airfoil curve being slightly higher than that for the rotating blade point ensemble. Notably, maximum rotating blade C_n at 13-m blade radius (C_n = 2.24) exceeded maximum stationary airfoil C_n (C_n = 1.41) by a factor of 1.59, due to the influence of rotational augmentation effects.

Comparing Figures 5 and 6, trends in the two-dimensional, nonrotating data are apparent and consistent with blade geometry. At the 7-m blade radius, two-dimensional, nonrotating C_n reached a maximum of 1.06, and at the

13-m station, it attained a maximum of 1.41. Increasing C_n maxima at greater blade radius is consistent with decreasing airfoil thickness ratio, and the accompanying delay in boundary layer separation as adverse pressure gradients were reduced.

Most significant for blade aerodynamics are differences between the two-dimensional, nonrotating airfoil and the three-dimensional, rotating blade. The 7-m blade radius (Figure 5) showed a difference of 1.47 between C_n maxima for the two-dimensional stationary airfoil and the three-dimensional rotating blade. At the 13-m radius (Figure 6), the difference between these two C_n maxima was 0.63 and significantly less than that inboard at the 7-m location. The C_n increment for three-dimensional rotating conditions relative to two-dimensional stationary conditions and the decrease in this increment with radial location is attributable to rotational augmentation and is consistent with previous measurements.[8,19]

Also identified above were differences in slope between the two-dimensional, nonrotating airfoil and the three-dimensional, rotating blade. Though not quantified, this difference was substantial at the 7-m blade radius (Figure 5). At the 13-m blade radius (Figure 6), this slope difference still was apparent but was less than that for the 7-m station. Similar slope increments and trends with respect to blade radial location have been noted in previous efforts.[8,19] Here, these phenomena can be attributed to three-dimensionality mediated by potential flow interactions acting in the blade root vicinity.

C. Surface Pressure Distributions

To understand the fluid dynamics underlying three-dimensional rotationally augmented blade C_n levels documented above, as well as the two-dimensional stationary airfoil reference datum, blade surface pressure distributions were examined for select C_n conditions. To do so, surface pressure data for three-dimensional rotationally augmented conditions were obtained from the same 157 one-minute Siemens 2.3-MW turbine data sets discussed above. Surface pressure data for the two-dimensional stationary airfoil reference cases were derived from Siemens proprietary wind tunnel testing databases.

These surface pressure data are shown in Figures 7 through 10, where Figure 8 and Figure 10 c_p distributions represent means computed from the one-minute data sets, and data in Figures 7 and 9 were acquired from two-dimensional wind tunnel experiments. In Figures 7 through 10, to avoid compromising Siemens proprietary data, pressure surface data have been omitted to conceal stagnation point c_p and thus eliminate any zero reference. For the same reason, tick marks and labels have been removed from the vertical axis, to eliminate any scaling information. However, zero references and vertical axis scaling are consistent for Figures 7 through 10, to enable comparisons of suction surface c_p distributions.

Figure 8 shows suction surface c_p distributions for rotating conditions at the 7-m blade radius, and Figure 7 shows the same data for two-dimensional stationary conditions as measured in a wind tunnel airfoil test. Wind tunnel data were not available for the airfoil section at the 7-m blade location, and instead wind tunnel data for the airfoil section corresponding to the 9-m radius were used. Between the 7-m and 9-m blade radii, the difference in airfoil thickness was approximately 5%.

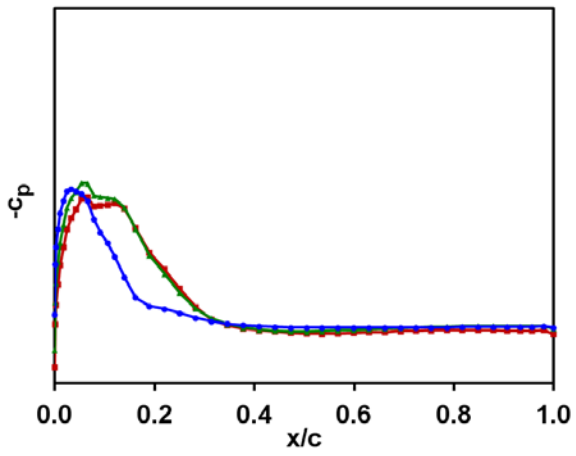

Figure 7. Suction surface c_p vs. x/c for two-dimensional stationary wind tunnel measurements.

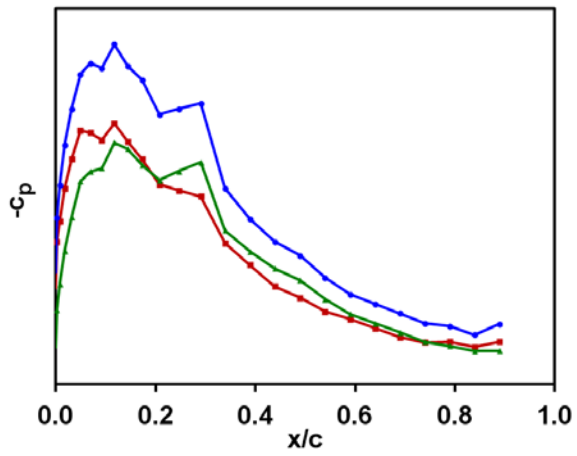

Figure 8. Suction surface c_p vs. x/c for three-dimensional rotating blade measurements at 7-m blade radius.

The three c_p distributions in Figure 8 correspond to data points in Figure 5 for which $C_n > 2.0$, and were selected as being representative of rotationally augmented conditions. Like the C_n data in Figure 5, the c_p data in Figure 8 also are mean data computed from one-minute data sets. Using the stagnation point location (not shown herein) for these three blade c_p distributions as a reference, the three two-dimensional airfoil c_p distributions in Figure 7 were identified as being at the same angles of attack (α).

In Figure 7, all three c_p distributions were similar and displayed attributes typical of two-dimensional airfoils at elevated α. Peak c_p magnitudes occurred near the leading edge, at x/c = 0.033 and x/c = 0.053. Aft of these locations, suction decreased rapidly with chord and began to level off in the range $0.314 \leq x/c \leq 0.378$. Downstream of this chord region, the surface pressure distribution was virtually flat, indicating that the boundary layer was separated over much of the aft portion of the airfoil suction surface.

Figure 8 shows suction surface pressure distributions for three-dimensional rotating conditions at the same angles of attack as the two-dimensional stationary c_p distributions in Figure 7. Significant differences between stationary two-dimensional (Figure 7) and rotating three-dimensional (Figure 8) conditions were apparent. In Figure 8, peak c_p magnitudes occurred at x/c = 0.117, approximately 0.05c to 0.08c aft of those in Figure 7. In addition, the Figure 8 peak c_p magnitudes exceeded those in Figure 7 by factors of 1.30 to 1.71. Finally, Figure 7 c_p magnitudes decreased steeply over the 0.15c to 0.25c aft of the peak location, and thereafter remained level over the rear 0.7c of the airfoil. In contrast, the Figure 8 c_p magnitudes decreased in pseudo-linear fashion from the peaks to the trailing edge vicinity, and level regions in the c_p distribution were virtually nonexistent, implying that separation was negligible, having been precluded by rotational augmentation of the blade boundary layer.

Figure 10 shows suction surface c_p distributions for rotating conditions at the 13-m blade radius, and Figure 9 shows the same data for two-dimensional stationary conditions as measured in a wind tunnel airfoil test. Wind tunnel data were not available for the airfoil section at the 13-m blade location, and wind tunnel data for the airfoil section corresponding to the 14-m radius were used instead. Between the 13-m and 14-m blade radii, the difference in airfoil thickness was approximately 2%.

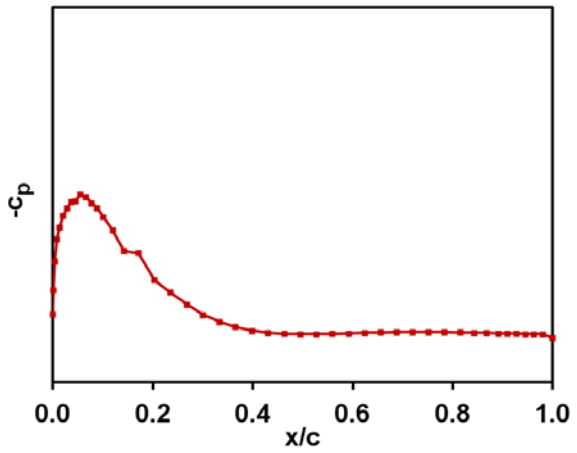

Figure 9. Suction surface c_p vs. x/c for two-dimensional stationary wind tunnel measurements.

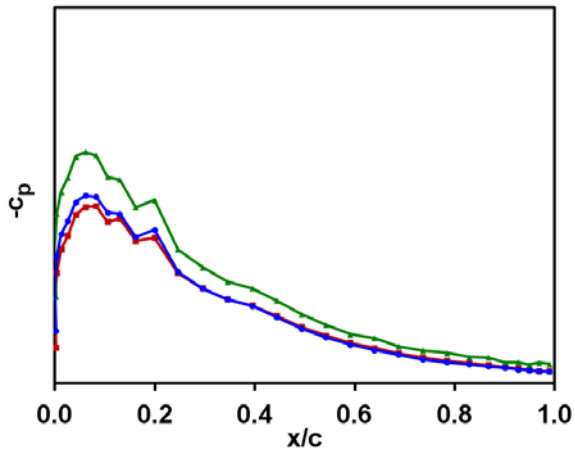

Figure 10. Suction surface c_p vs. x/c for three-dimensional rotating blade measurements at 13-m blade radius.

The three Figure 10 c_p distributions correspond to Figure 6 data points where $C_n > 1.5$ and were chosen as typical of rotationally augmented conditions. Like the C_n data in Figure 6, the c_p data in Figure 10 also are mean data extracted from one-minute data sets. Using the location of the stagnation point (not shown herein) for the three blade c_p distributions, the two-dimensional airfoil c_p distribution in Figure 9 was identified as corresponding to the same α.

In Figure 9, the airfoil c_p distribution was consistent with those produced by two-dimensional airfoils at elevated α. Peak c_p magnitude occurred near the leading edge, at x/c = 0.055. Downstream of this location, suction declined progressively with chord and began to level off at approximately 0.40c. Downstream of 0.40c, the surface pressure distribution was virtually flat, implying that boundary layer separation dominated the aft region of the airfoil suction surface.

Figure 10 shows suction surface c_p distributions for three-dimensional rotating conditions at the same α as the stationary airfoil c_p distribution in Figure 9. Here, as at the 7-m blade radius, differences existed between two-dimensional stationary conditions (Figure 9) and three-dimensional rotating conditions (Figure 10). In Figure 10, peak c_p magnitudes occurred at x/c = 0.055c and 0.082c, which were aft of the peak at 0.061c in Figure 9. Figure 10 peak c_p magnitudes were 94% to 123% of that in Figure 9. Finally, Figure 9 c_p magnitudes dropped off through 0.05c to 0.40c downstream of the peak location, and then remained virtually flat over the aft 0.6c. In contrast, c_p magnitudes in Figure 10 decreased in pseudo-linear fashion from the suction peaks to the neighborhood of the trailing edge vicinity. As at the 7-m blade radial station, flat c_p distribution regions were not apparent in the Figure 10 rotating blade c_p data, indicating that separation was similarly insignificant, due to rotational augmentation of the blade boundary layer.

D. Rotational Augmentation Context

In the current effort, clear differences were apparent between two-dimensional stationary airfoil performances and three-dimensional rotating blade responses at both the 7-m and 13-m blade radius locations. However, the most pronounced differences occurred at the inboard location at 7 m, with respect to: 1) C_n increment for three-dimensional rotating conditions relative to two-dimensional stationary conditions, 2) Peak c_p magnitude, 3) Peak c_p chordwise location, and 4) c_p distribution shape aft of the peak. This radial variation in rotational augmentation is consistent with radial variation in the ratio c/r, as shown previously by Snel et al.[18]

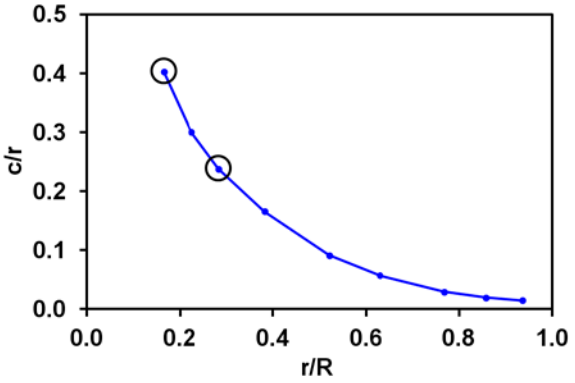

Figure 11. (c/r) vs. (r/R) for Siemens 2.3-MW rotor used in current study.

Figure 11 shows a plot of c/r for the Siemens 2.3-MW turbine blade. Across the entire blade, c/r varied between 0.40 at 0.17R, to 0.02 at 0.94R. The 7 m and 13 m blade radius locations analyzed in the current work are identified by circles, where c/r = 0.40 and 0.24, respectively. That rotational augmentation observed at these two radial locations is consistent with previous research. Analyses of UAE Phase VI[8] and MEXICO[19] data showed that rotational augmentation influences were prominent down to c/r = 0.17, and that rotationally augmentation was detectable for c/r levels as low as c/r = 0.1.

IV. Conclusions

The current work is aimed at exploiting data acquired from the Siemens 2.3-MW turbine at NREL's National Wind Technology Center to improve fundamental comprehension of rotationally augmented blade aerodynamic response. In particular, analyses were directed at determining whether thick, flatback airfoil sections significantly alter rotational augmentation. The current effort supports the following conclusions regarding rotational augmentation on megawatt-scale turbines using thick, flatback airfoils:

- Rotating blade aerodynamic time-averaged forces are amplified by factors as high as 2 to 3, relative to stationary two-dimensional conditions.
- Rotating blade time-averaged leading edge suction nearly doubles under some conditions, again relative to stationary, two-dimensional conditions.
- Rotating blade time-averaged pressure distributions are pseudo-linear, and pressure recovery indicates greatly reduced boundary layer separation, compared to stationary, two-dimensional conditions.
- Rotationally augmented blade response persisted as indicated by mean statistics, though inflows at the field test site are highly turbulent.
- Prevalence and intensity of rotational augmentation across the blade radius is consistent with that observed for blades having lower thickness ratios and conventional trailing edges, and is not impeded by elevated airfoil thickness or flatback design.

The current work provides novel insights into rotational augmentation on megawatt-scale turbines using thick, flatback airfoils. These findings provide a solid foundation for future research in two separate but equally important

directions. First, the understanding and data furnished herein can be used as a basis for validating and improving post-stall models in aeroelastic design codes. Second, the time-average analyses used in the current work can be enhanced with time-varying data and analyses to characterize and better understand fatigue loading generated by rotationally augmented blade flows.

References

[1]Himmelskamp, H., "Profiluntersuchungen an einem umlaufenden Propeller," Dissertation, Gottingen 1945; Mitt. Max-Planck-Institut fur Stromungsforschung Gottingen Nr. 2, 1950.

[2]Banks, W., and Gadd, G., "Delaying Effect of Rotation on Laminar Separation," *AIAA J.*, v. 1, n. 4, Apr. 1963, pp. 941-942.

[3]McCroskey, W., and Yaggy, P., "Laminar Boundary Layers on Helicopter Rotors in Forward Flight," *AIAA J.*, v. 6, n. 10, Oct. 1968, pp. 1919-1926.

[4]McCroskey, W. J., "Measurements of Boundary Layer Transition, Separation and Streamline Direction on Rotating Blades," NASA TN D-6321, Apr. 1971.

[5]Madsen, H., and Christensen, H., "On the Relative Importance of Rotational, Unsteady and Three-Dimensional Effects on the HAWT Rotor Aerodynamics," *Wind Engineering*, v. 14, n. 6, 1990, pp. 405-415.

[6]Barnsley, M., and Wellicome, J., "Wind Tunnel Investigation of Stall Aerodynamics for a 1.0 m Horizontal Axis Rotor," *Journal of Wind Engineering and Industrial Aerodynamics*, v. 39, 1992, pp. 11-21.

[7]Ronsten, G., "Static Pressure Measurements on a Rotating and a Non-Rotating 2.375 m Wind Turbine Blade. Comparison with 2D Calculations," *Journal of Wind Engineering and Industrial Aerodynamics*, v. 39, 1992, pp. 105-118.

[8]Schreck, S., and Robinson, M., "Rotational Augmentation of Horizontal Axis Wind Turbine Blade Aerodynamic Response," *Wind Energy*, v. 5, n. 2/3, pp. 133-150, Apr.-Sep. 2002.

[9]Schreck, S., and Robinson, M., "Boundary Layer State and Flow Field Structure Underlying Rotational Augmentation of Blade Aerodynamic Response," *Journal of Solar Energy Eng.*, v. 125, pp. 448-456, November 2003.

[10]Schreck, S., and Robinson, M., "Structures and Interactions Underlying Rotational Augmentation of Blade Aerodynamic Response," AIAA-2003-0520, January 2003.

[11]Schreck, S., Sørensen, N., and Robinson, M., "Aerodynamic Structures and Processes in Rotationally Augmented Flow Fields," *Wind Energy*, v. 10, n. 2, March/April 2007, pp. 159-178.

[12]Schreck, S., and Robinson, M., "Tip Speed Ratio Influences on Rotationally Augmented Boundary Layer Topology and Aerodynamic Force Generation," AIAA-2004-0663, January 2004.

[13]Schreck, S., and Robinson, M., "Unsteadiness in HAWT Blade Aerodynamic Forces and Flow Field Structures During Rotational Augmentation," AIAA-2005-0776, January 2005.

[14]Schreck, S., "Rotationally Augmented Flow Structures and Time Varying Loads on Turbine Blades," AIAA-2007-0627, January 2007.

[15]Schreck, S., "Spectral Content and Spatial Scales in Unsteady Rotationally Augmented Flow Fields," 2007 Science of Making Torque from Wind Conference, Journal of Physics: Conference Series **75** (2007) 012024, DOI: 10.1088/1742-6596/75/1/012024, August 2007.

[16]Medina, P., Singh, M., Johansen, J., Fingersh, L., Schreck, S., "Inflow Characterization and Aerodynamic Measurements on a SWT-2.3-101 Wind Turbine," AIAA-2012-2030.

[17]Strike, J., Hind, M., Singh, M., Naughton, J., Wilson, M., and Whitmore, S., "Unsteady Surface Pressure Reconstruction on an Oscillating Airfoil Using the Wiener Deconvolution Method," 27th AIAA Aerodynamic Measurement Technology and Ground Testing Conference, Chicago, IL, 2010.

[18]Snel, H., Houwink, R., and Bosschers, J., "Sectional Prediction of Lift Coefficients on Rotating Wind Turbine Blades in Stall," ECN-C--93-052, December 1994.

[19] Schreck, S., Sant, T., and Micallef, D., "Rotational Augmentation Disparities in the MEXICO and UAE Phase VI Experiments," Proceedings of the 2010 Torque from Wind Conference, Crete, Greece, June 28-30, 2010.